Hierarchical reference theory study of the lattice restricted primitive model

A. Brognara,[1] A. Parola,[2] and L. Reatto[1]
[1]*Dipartimento di Fisica, Università di Milano and Instituto Nazionale per la Fisica della Materia, Via Celoria 16, 20133 Milano, Italy*
[2]*Dipartimento di Scienze, Università dell'Insubria and Istituto Nazionale per la Fisica della Materia, Via Valleggio 11, Como, Italy*
(Received 23 October 2001; published 20 June 2002)

A three dimensional model of point charges, named lattice restricted primitive model (LRPM), is investigated by using the hierachical reference theory of fluids. This approach, which generalizes the momentum renormalization group technique, is shown to capture the physics of the model and provides a quantitative description of the phase diagram. The comparison with recent numerical simulations and with other theoretical approaches is discussed both for the LRPM and for the Blume-Capel model, which can be seen as a screened version of LRPM. The nonuniversal crossover region close to the tricritical point is also discussed.

DOI: 10.1103/PhysRevE.65.066113 PACS number(s): 64.60.−i, 05.50.+q, 05.10.Cc

I. INTRODUCTION

Criticality in ionic fluids has been a subject of great debate and study in the last century [1,2]. In fact, the long range nature of the interatomic potential makes this problem very difficult to deal with and there is not even general consensus on many key issues, such as the universality class of the liquid-vapor critical behavior in ionic fluids. This anomalous aspect of the Coulomb criticality is further supported by recent experimental results [3] that have shown that both Ising-like and mean-field-like criticality can be observed for these systems. Although Ising criticality is generally believed to represent the asymptotic behavior, the experimental evidence requires an explanation of the anomalously large crossover detected in electrolytes.

The simplest theoretical model able to capture the main features of ionic fluids is the restricted primitive model (RPM). This model is a symmetric mixtures of positive and negative charged hard spheres of equal diameters immersed in a neutral fluid of dielectric constant D. From the first pioneering work of Debye and Hückel [4] several approximations and theories have been introduced to treat the RPM. However, the first evidence of criticality in the RPM was shown by Stell and co-workers only in 1976 [5] where, by using a mean spherical approximation (MSA), they found a coexistence curve that ends at a critical point. They also showed that the details of the coexistence curve strongly depend on the approximation employed so, in order to better describe these properties, various other approaches have been developed to treat ionic systems. Using a mean-field approximation, Fisher and co-workers concluded that in order to obtain realistic values for ρ_c and T_c it was necessary to include Bjerrum association and dipole-charge interaction [6,7].

Recently, in an attempt to better understand the critical properties of the RPM, attention has been attracted by the lattice version of this model (LRPM) [1,2]. However, the phase diagram of the lattice model contains features that are absent in the continuous case. In fact, above the coexistence region, where a disordered and a charge modulated phase can coexist at two different densities, the phase diagram displays a Néel line of critical points which is absent in the RPM.

The thermodynamic properties of the LRPM have also been investigated by a number of approximate theories. In particular, we mention the MSA study of Høye and Stell [8] and the field theoretical methods developed by Ciach and Stell [9,10], which addressed the interesting problem of the nature of the differences between the phase diagram of the RPM and LRPM. However, the critical properties extracted from all these theories do not go beyond mean-field level or mean spherical approximation [9,11] and are not in very good agreement with simulation results [12,13]. Recently this model has also been studied by using the self-consistent Ornstein-Zernike approximation (SCOZA) by Grollau *et al.* [14].

In order to provide a theory capable of improving the agreement with simulation results, we present an approach to LRPM based on the hierarchical reference theory (HRT) implementation of the renormalization group (RG). Originally developed to describe properties of simple fluids, this theory has been later extended to treat lattice models [15] and fluid mixtures [16].

The main advantage of HRT approach is that, starting only from the microscopic interaction between constituents, it allows one to derive an infinite set of coupled differential equations, which is formally exact. These equations describe the evolution of the thermodynamic quantities when fluctuations are gradually included and give rise to the correct RG structure, which clearly identifies the universality class and the critical properties of the model. However, in order to quantitatively analyze this set of equations, an approximate relation (closure relation) that allows one to reduce the infinite set to a finite number of equations must be introduced.

This paper is organized as follow. In Sec. II we derive a formulation of HRT, which is particularly suitable to treat symmetric mixtures. The closure relation employed for the integration of the first equation of the hierarchy is also discussed. In Sec. III we describe the application to two lattices models. The first one is the Blume-Capel model, which involves only nearest neighbor interactions and is useful as a check of the approximations employed. Then we discuss the application to the LRPM, which is the main subject of this work. In Sec. IV numerical results of the integration of HRT

equations for the two models are presented and finally Sec. V contains conclusions and perspectives.

II. HRT EQUATIONS FOR SYMMETRIC MIXTURES

In this section we review the application of the HRT formalism to binary mixtures on a lattice [16,17]. We start by considering a system whose constituents interact through a two-body central potential $v_{i,j}(r)$. Here the subscripts stand to label the species. The first step in the derivation of HRT equations is to separate the interacting potential into two parts:

$$v_{i,j}(r)=v_{i,j}^{R}(r)+w_{i,j}(r), \tag{1}$$

where $v_{i,j}^{R}$ is the reference term whose properties are assumed known and $w_{i,j}(r)$ represents the ''perturbation term'' that includes the long range part of the interaction.

In full analogy with the one-component case, the separation (1) allows one to derive a perturbative expansion, for the free energy. Here we report only the first term of this expansion, which includes the resummation of the infinite one loop diagrams of the perturbative series:

$$-\frac{\beta A}{V}=-\frac{\beta A_R}{V}-\frac{1}{2}\rho_i\phi_{i,i}(r=0)+\frac{1}{2}\rho_i\rho_j\phi_{i,j}(k=0) -\frac{1}{2}\int\frac{d^dk}{(2\pi)^d}\mathrm{Tr}[\ln\{1-F_R(k)\phi(k)\}]+\cdots. \tag{2}$$

The other terms are related to higher loop contributions. In Eq. (2) we have defined $\phi_{i,j}(k)=-\beta w_{i,j}(k)$, $F_{Ri,j}(k)$ is the correlation function of the reference system, matrix notation has been employed and summation over repeated indices is understood. The integrations are extended to the full Brillouin zone.

Clearly, a perturbative expansion such as Eq. (2) breaks down near phase boundaries and cannot be used as a starting point for a realistic description of the phase diagram of the model. Rather, in order to include, in the free energy, the contribution due to the perturbation term a momentum space renormalization group approach is implemented. This can be accomplished by first defining a sequence of systems characterized by a lower cutoff, labeled by p, on fluctuations. From now on we simply refer to each of these systems as the *p system*; this means to restrict the domain of integration in Eq. (2) to a region $\mathcal{B}_p$. Varying p this region must span the full momentum space. The actual shape of the domain $\mathcal{B}_p$ will be specified later taking into account the specific features of the symmetry breaking mechanism that occur at the transition. The introduction of cutoff on fluctuations can be conveniently performed by introducing a potential with a sharp cutoff at long wavelength defined as

$$w_{ij}^{p}(k)\begin{cases} w_{i,j}(k), & k\in\mathcal{B}_p \\ 0, & k\notin\mathcal{B}_p. \end{cases} \tag{3}$$

The generality of the perturbative expansion (2) allows one to obtain the properties of the system with a cutoff $p-\delta p$ considering the *p system* as reference. For this purpose it is enough to consider the one-loop contributions shown in Eq. (2). In this way it is possible to derive an exact infinite hierarchy of equations, which describes the evolution of the thermodynamic properties of the system when fluctuations are gradually included. The resulting differential equation for the free energy is then given by

$$-\frac{d}{dp}\mathcal{A}^p=\frac{1}{2}\int_{\Sigma_p}\frac{d\omega_k}{(2\pi)^d}\mathrm{Tr}\{\ln[1+\mathcal{F}^p(k)\phi(k)]\} \tag{4}$$

$$=\frac{1}{2}\int_{\Sigma_p}\frac{d\omega_k}{(2\pi)^d}\ln\det[1+\mathcal{F}^p(k)\phi(k)]. \tag{5}$$

Here Σ_p is the contour surface of the region $\mathcal{B}_p$. It should be noted that this evolution equation is exact because the higher order loop diagrams do not contribute. In Eq. (5), in order to deal with continuous quantities, a modified free energy density $\mathcal{A}$ and correlation function $\mathcal{F}(k)$, including the mean field terms have been defined,

$$\mathcal{A}^p=-\frac{\beta A^p}{V}-\frac{1}{2}\rho_i\int d^dk[\phi_{i,i}(k)-\phi_{i,i}^p(k)] +\frac{1}{2}\rho_i\rho_j[\phi_{i,j}(0)-\phi_{i,j}^p(0)], \tag{6}$$

$$-(\mathcal{F}^{-1})_{i,j}^p(k)=\mathcal{C}_{i,j}^p(k)=c_{i,j}^p(k)+\phi_{i,j}(k)-\phi_{i,j}^p(k). \tag{7}$$

Unfortunately, Eq. (5) is not closed because the two point correlation function $\mathcal{F}^p(k)$ is not simply related to the free energy and its evolution can be expressed in terms of the three- and four-point correlation functions. The formal structure of the hierarchy has been discussed in Ref. [16] and will not be repeated here. In the case of symmetric mixtures with $\phi_{1,1}=-\phi_{1,2}=\phi$, the whole hierarchy simplifies. In fact,

$$\det[1+\mathcal{F}^Q(k)\phi(k)]=1+[\mathcal{F}_{1,1}(k)+\mathcal{F}_{2,2}(k) -2\mathcal{F}_{1,2}(k)]\phi(k)=1+\mathcal{F}_{cc}(k)\phi(k), \tag{8}$$

where $c=\rho_1-\rho_2$ and we have introduced the concentration correlation function $\mathcal{F}_{cc}(k)$. Using this expression the evolution equation for the free energy can be written in the simplified form

$$-\frac{d}{dp}\mathcal{A}^p=\frac{1}{2}\int_{\Sigma_p}\frac{d\omega_k}{(2\pi)^d}\ln[1+\mathcal{F}_{cc}^p(k)\phi(k)]. \tag{9}$$

In this equation the density correlation function does not appear. This is not a peculiarity of the free energy equation of the hierarchy but it can be shown that in the full hierarchy only concentration correlations are involved. In other words, for symmetric mixtures with $\phi_{1,1}=-\phi_{1,2}$ the density correlation functions are fully decoupled from the hierarchy. As a consequence, any phase transition occurring in such a model must be accompanied by some singularity in the concentration fluctuations; otherwise, Eq. (9) would lead to a fully

regular thermodynamics. It is important to remark here that this is not an approximation, because the infinite set of equations is exact.

Closure relation

As already stated, the evolution equation (9) is not closed because $\mathcal{F}^p_{cc}(k)$ is related to higher order correlation functions and so a quantitative study of this equation cannot be performed. In order to obtain results for nonuniversal quantities, a closure relation able to account approximatively for the integration of the remaining set of equations must be introduced. In the following, we describe how a closure relation can be implemented. In the discussion we will adopt a magnetic language and so charges and vacancies are identified with a three-state spin defined at every lattice site coupled by the antiferromagnetic interaction $w(r)$.

First of all it is known that at the mean-field level [11,12], the relevant fluctuations of the system are those around $\boldsymbol{k}=\boldsymbol{\pi}$. This is further supported by simulation results [12,13] that suggest the presence in the phase diagram of a Néel line characterized by the divergences of $\mathcal{F}_{cc}$ at the wave vector $\boldsymbol{k}=\boldsymbol{\pi}$. In order to relate these fluctuations to the thermodynamics, it is necessary to introduce the appropriate sum rule in full analogy with the treatment of ferromagnetic transition [15]. This can be achieved by introducing an external staggered magnetic field that tends to create an antiferromagnetic order. It is also convenient to perform a Legendre transformation, which allows to eliminate the density dependence in favor of the chemical potential,

$$\Omega^p(\mu,h)=\mathcal{A}^p(\rho,h)+\mu\rho, \tag{10}$$

where h and μ are the staggered field and the chemical potential measured in units of k_BT, while $\rho=\rho_1+\rho_2$ is the total density. In this way the compressibility sum rule takes the simple form

$$\left.\frac{\partial^2\Omega^p}{\partial h^2}\right|_{\mu=\text{const}}=\mathcal{F}^p_{cc}(\boldsymbol{k}=\boldsymbol{\pi}). \tag{11}$$

It is now convenient to express the thermodynamics in terms of the staggered magnetization $\varphi=\Sigma_i(-1)^iS_i$ instead of the magnetic field. This leads to the further definitions

$$G^p(\mu,\varphi)=\Omega^p(\mu,h)-h\varphi, \tag{12}$$

with

$$\rho=\frac{\partial G}{\partial\mu}, \tag{13}$$

$$\varphi=\frac{\partial\Omega}{\partial h}. \tag{14}$$

With this substitution, Eq. (9) takes the form

$$\frac{d}{dp}G^p=-\frac{1}{2}\int_{\Sigma_p}\frac{d\omega_k}{(2\pi)^d}\ln\left[1-\frac{\phi(k)}{\mathcal{C}^p_{cc}(k)}\right], \tag{15}$$

where the integration runs over the surface Σ_p that, varying the label p, spans the full first Brillouin zone of the lattice. The direct correlation function is defined as

$$\mathcal{C}^p_{cc}(k)=-\frac{1}{\mathcal{F}^p_{cc}(k)} \tag{16}$$

and the exact sum rule reads

$$\mathcal{C}^p_{cc}(\boldsymbol{k}=\boldsymbol{\pi})=\frac{\partial^2G^p}{\partial\varphi^2}\equiv\xi^p, \tag{17}$$

where ξ^p is simply related to the staggered susceptibility of the p system. We now discuss the application of Eq. (15) to the study of two simple cubic lattice models. In both these cases the interacting potential depends only on the function

$$\gamma_k=\frac{1}{3}\sum_{i=1}^{3}\cos k_i. \tag{18}$$

The surfaces Σ_p of the integration domain are defined as

$$\Sigma_p=\{k;|\gamma_k|<|p|\}\quad\text{with}\quad -1<p<0. \tag{19}$$

Starting from $p=0$, this surface spans the whole first Brillouin zone moving simultaneously to the center ($\boldsymbol{k}=\boldsymbol{0}$) and to the corner ($\boldsymbol{k}=\boldsymbol{\pi}$) of this region where critical fluctuations may develop. This choice has the advantage of leading to a stable integration algorithm. This, with the compressibility rule (17), suggests the following parametrization for the concentration correlation function:

$$\mathcal{C}^p_{cc}(k)=\xi_0-\phi(k)+\alpha_p\gamma_k. \tag{20}$$

Here ξ_0 (independent of k) is the staggered susceptibility of the reference system which is just a two-component lattice gas in a staggered magnetic field and α_p is a function that must be determined according to the compressibility sum rule at $\boldsymbol{k}=\boldsymbol{\pi}$,

$$\alpha_p=\xi_0-\xi^p-\phi(k=\pi). \tag{21}$$

A similar parametrization of the two-body correlations has also been proposed by Grollau *et al.* [14] for the integration of SCOZA equations.

The grand canonical partition function of the reference system in the presence of a staggered magnetic field can be calculated analytically; and in the symmetric case its expression is given by

$$\Omega=\ln(1+2z\cosh h)\quad\text{with}\quad z=e^{\mu}. \tag{22}$$

Using the relations (11), (12), and (16) we obtain the following expression for the staggered susceptibility of the reference:

$$\xi_0 = -\frac{(1+2z\cosh\beta h)^2}{2z(\cosh h+2z)}, \tag{23}$$

with

$$h = \ln\frac{\varphi+\sqrt{\varphi^2+4z^2(1-\varphi^2)}}{2z(1-\varphi)}. \tag{24}$$

Before discussing the numerical solution of the partial derivative equation we point out that the closure relation (20) does not automatically fulfill the core condition leading to the possibility of multiple occupancy of a lattice site. In our approximation this condition is verified only for the reference system at the beginnings of the integration. Usually [16], neglecting the core condition does not severely affect the numerical determination of the critical points and the shape of the coexistence curve, and, of course, does not modify the critical behavior predicted by HRT.

Finally the dielectric function is simply related to the two-body correlations by the relation

$$\epsilon(k) = [1-\mathcal{F}_{cc}(k)\phi(k)]^{-1} = 1-\frac{\phi(k)}{\xi_0+\alpha_p\gamma_k}. \tag{25}$$

In the case of Coulomb potential $\phi(k)$ behaves like k^{-2} for $k\to 0$, while the evolution equation (15) forces $\xi_0+\alpha_p\gamma_k$ to be always negative. This implies that with our closure

$$\epsilon(k) \sim_{k\to 0} \frac{1}{k^2}, \tag{26}$$

which coincides with the perfect screening condition.

III. NUMERICAL SOLUTION OF HRT EQUATIONS

In this section we discuss the application of the theory developed in Sec. II to two lattice models by detailing the numerical solution of the first equation of the Hierarchy (15) with the closure relation (17), (20), and (21).

A. Application to the Blume-Capel model

As a first application of the formalism just developed, we study the Blume-Capel model which is a generalization of the Ising model where spins can assume three distinct values 1 for one specie, -1 for the other specie, and 0 for holes. Its Hamiltonian is given by

$$H = -J\sum_{\langle i,j\rangle} S_iS_j - h\sum_i (-1)^i S_i \tag{27}$$

and is a special case of the Blume-Emery-Griffiths Hamiltonian that contains an extra term $-K\Sigma_{\langle i,j\rangle}S_i^2S_j^2$ and has been applied to the study of the ^{3}He-^{4}He mixtures.

In Fourier space, the interacting potential is

$$\phi(k) = \lambda\gamma_k \quad \text{with} \quad \lambda = \frac{6J}{kT} \tag{28}$$

and the closure relation (20) together with Eq. (17) becomes

$$\mathcal{C}_{cc}^p(k) = (1+\gamma_k)\xi_0 - \gamma_k\xi^p. \tag{29}$$

Inserting this relation (29) into expression (15) we obtain the following evolution equation:

$$\frac{\partial G^p}{\partial p} = -\frac{1}{2}D_p\left[\ln\left(1+\frac{\phi_p(\gamma_k=p)}{\mathcal{C}_{cc}^p(\gamma_k=p)}\right) + \ln\left(1+\frac{\phi_{-p}(\gamma_k=-p)}{\mathcal{C}_{cc}^{-p}(\gamma_k=-p)}\right)\right] \tag{30}$$

$$= -\frac{1}{2}D_p\ln\left[\frac{\xi_0^2-p^2\alpha_p^2}{\xi_0^2-p^2(\lambda-\alpha_p)^2}\right], \tag{31}$$

where we have introduced the density of states defined as

$$D_p = \int_{\mathcal{B}}\frac{d^3k}{(2\pi)^3}\,\delta(p-\gamma_k). \tag{32}$$

The numerical solution of Eq. (31) can be more easily achieved once it has been transformed into a quasilinear form

$$\frac{\partial^2 v_p}{\partial\varphi^2} = A(p,v_p,\varphi)\frac{\partial v_p}{\partial t} + B(p,v_p,\varphi) \quad \text{with} \quad t=\ln(1+p). \tag{33}$$

This transformation can be made by defining a new variable v_p as

$$e^{p^2v_p} = x = \frac{\xi_0^2-p^2\alpha_p^2}{\xi_0^2-p^2(\lambda-\alpha_p)^2} \tag{34}$$

and taking two derivatives in φ on both sides of Eq. (31). Here we only report the results for the coefficients $A(p,v_p,\varphi), B(p,v_p,\varphi)$ of the quasilinear form

$$A(p,v_p,\varphi) = -\frac{2x}{D_p(1+p)}\frac{\partial\alpha_p}{\partial p}, \tag{35}$$

$$B(p,v_p,\varphi) = \frac{2}{D_pp^2}\left(\frac{\partial\alpha_p}{\partial p}+2xpv_p\frac{\partial\alpha_p}{\partial x}\right). \tag{36}$$

Where the partial derivatives of α_p are given by

$$\frac{\partial\alpha_p}{\partial p} = -\frac{(1-x)\xi_0^2}{p\sqrt{p^4x\lambda^2+p^2(1-x)^2\xi_0^2}}, \tag{37}$$

$$\frac{\partial\alpha_p}{\partial x} = -\frac{\lambda}{(1-x)^2}+\frac{p^2(1+x)\lambda^2}{2\sqrt{p^4x\lambda^2+p^2(1-x)^2\xi_0^2}(1-x)^2}. \tag{38}$$

The boundary condition at $\varphi=0$ reflects the symmetry of the system under the substitution of $\varphi\leftrightarrow-\varphi$. This implies that

$$v_p(-\varphi) = v_p(\varphi) \tag{39}$$

at every stage of the integration. The boundary condition at $\varphi=1$ instead can be derived from the expression of the correlation function for the reference system, which implies

$$\lim_{\varphi\to 1}\xi_0=-\infty. \tag{40}$$

This condition is maintained at every step of the integration and in terms of v_p can be written as

$$v_p(\varphi=1)=0. \tag{41}$$

The integration of Eq. (33) with the boundary conditions (39) and (41) has been performed using an implicit Predictor Corrector algorithm [18,19].

B. Application to the lattice restricted primitive model

The discussion of the LRPM proceeds along the same lines of the Blume-Capel model. As interacting potential in Fourier space, we use the expression

$$\phi(k)=\lambda\frac{1}{1-\gamma_k}\quad\text{with}\quad\lambda=\frac{2\pi}{3}\frac{q^2}{Dk_BT}, \tag{42}$$

which is the solution of the lattice Laplace equation. In real space Eq. (42) correctly reproduces the Coulomb potential only at large distances. In order to partially eliminate the self-interaction introduced by a nonvanishing contribution on site, we shift the potential by a constant in k space [9]. This is equivalent to a redefinition of the chemical potential. We choose the constant as λ so that the interacting potential becomes

$$\phi(k)=\lambda\frac{1}{1-\gamma_k}-\lambda=\lambda\frac{\gamma_k}{1-\gamma_k}, \tag{43}$$

leading to the explicit expressions for α_p and $\mathcal{C}^p_{cc}(k)$

$$\alpha_p=-\xi^p+\xi_0+\lambda/2, \tag{44}$$

$$\mathcal{C}^p_{cc}(k)=(1+\gamma_k)\xi_0-\gamma_k\xi^p-\frac{\lambda}{2}\gamma_k\frac{1+\gamma_k}{1-\gamma_k}. \tag{45}$$

Using the same integration surface of the Blume-Capel model, the evolution equation can be written as

$$\frac{\partial G^p}{\partial p}=-\frac{1}{2}D_p\left[\ln\left(1+\frac{\phi_p(\gamma_k=p)}{\mathcal{C}^p_{cc}(\gamma_k=p)}\right)+\ln\left(1+\frac{\phi_{-p}(\gamma_k=-p)}{\mathcal{C}^{-p}_{cc}(\gamma_k=-p)}\right)\right] \tag{46}$$

$$=-\frac{1}{2}D_p\left[\ln\frac{\xi_0^2-\alpha_p^2p^2}{(\xi_0^2-\alpha_p^2p^2)-2\lambda\dfrac{p^2}{1-p^2}\xi^p}+\ln(1-p^2)\right]. \tag{47}$$

By the substitution

$$1-p^2-e^{-p^2v_p}=y=\frac{2\lambda p^2\xi^p}{(\xi_0^2-\alpha_p^2p^2)}, \tag{48}$$

the evolution equation can be cast in the quasilinear form (33). The steps of the derivation are the same as before, the only difference here being that the double derivation with respect to φ allows one to eliminate the term $\ln(1-p^2)$, which becomes singular at the end of the integration. Here we only quote the coefficients of the quasilinear form

$$A(p,v_p,\varphi)=-\frac{2e^{-p^2v_p}}{D_p(1+p)}\frac{\partial\alpha_p}{\partial p}, \tag{49}$$

$$B(p,v_p,\varphi)=\frac{2}{D_pp^2}\left[\frac{\partial\alpha_p}{\partial p}-2p\frac{\partial\alpha_p}{\partial y}(1-e^{-p^2v_p}v_p)\right]. \tag{50}$$

where the partial derivatives of α_p are given by

$$\frac{\partial\alpha_p}{\partial p}=\frac{\xi_0^2y}{p\sqrt{\lambda^2p^4+p^2y(y\xi_0^2-2\lambda p^2\xi_0-\lambda^2p^2)}}, \tag{51}$$

$$\frac{\partial\alpha_p}{\partial y}=-\frac{\lambda}{y^2}+p^2\lambda\frac{2\lambda-\lambda y-2y\xi_0}{2y^2\sqrt{\lambda^2p^4+p^2y(y\xi_0^2-2\lambda p^2\xi_0-\lambda^2p^2)}}. \tag{52}$$

The boundary conditions for the integration variable are given by

$$v_p(\varphi)=v_p(-\varphi), \tag{53}$$

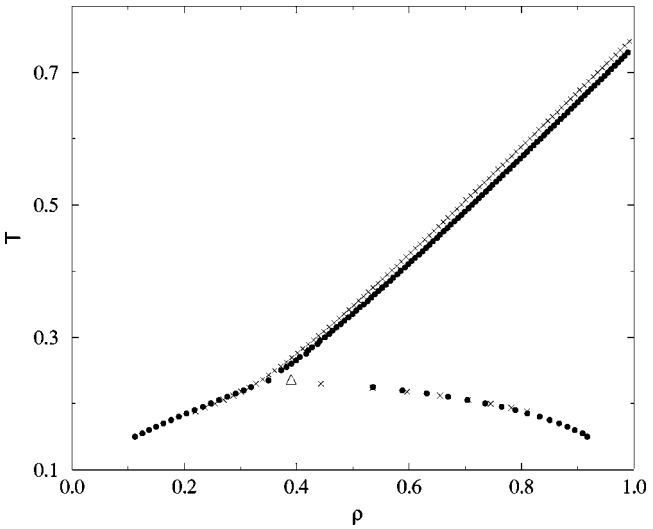

FIG. 1. Phase diagram in the $T-\rho$ plane for the Blume-Capel model. Temperatures are in units of 6 J/k_B. Circles, HRT results; crosses, results of SCOZA of Grollau *et al.* [23]. The triangle shows the tricritical point of Ref. [20].

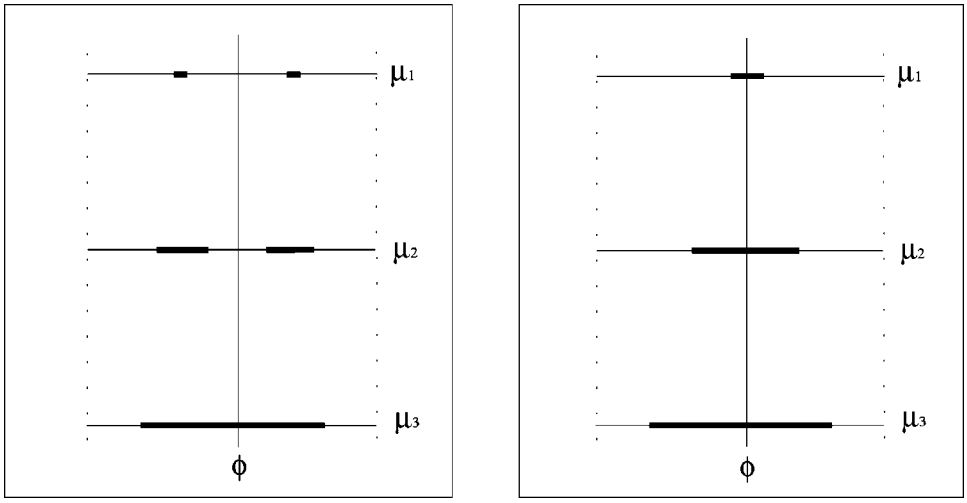

FIG. 2. Schematic representation of criticality below and above T_t. The wider lines delimit regions on staggered magnetization axis where $\mathcal{C}^{p=-1}(\boldsymbol{k}=\boldsymbol{\pi})=0$. As shown, for $T<T_t$ (figure on the left, $\mu=\mu_1$) transitions begin in regions away from $\varphi=0$. Increasing the chemical potential ($\mu_2>\mu_1$) this region enlarges and can include the origin ($\mu_3>\mu_2$). At temperatures higher than T_t instead (figure on the right) transitions always include $\varphi=0$.

$$v_p(\varphi=1)=-\frac{\ln(1-p^2)}{p^2}. \tag{54}$$

IV. RESULTS

The numerical integration of the first equation of HRT described in the sections herebefore allows one to determine several physically interesting quantities for the two lattice models introduced above. Simulations [12,13,20,21] and theoretical results [9,14] indicate that the phase diagram of both these models is characterized by a liquid-gas coexistence curve ending at a tricritical point, where a Neél line of critical points starts. However, before showing the numerical results, we briefly discuss how phase transitions may be detected. First of all we start considering the Néel line. On the left side of this line (see Fig. 1) the system is in a uniform paramagnetic phase. However, by increasing the chemical potential μ (or, equivalently, increasing the density of the system) antiferromagnetic order may appear; these two regions of the phase diagram are separated by the Néel line where the system undergoes a second order phase transition. As stated in Sec. II A, this transition is characterized by the divergence of the staggered susceptibility, i.e., by the vanishing of the function $\mathcal{C}_{cc}(k=\pi)$ at $\varphi=0$, and so it is possible to detect the points of the Néel line simply by looking at the vanishing of this function at the end of the integration. From the general theory of the tricritical points [22] it is known that along the Neél line the critical behavior is described by the Ising critical exponents. At the tricritical point, instead critical exponents have classical values in three dimensions. It can be verified that HRT equations [16] correctly reproduce this scenario.

Detecting points of the liquid-gas coexistence curve instead is a much more difficult task. In fact below the tricritical point the liquid-vapor coexistence curve is defined by a discontinuity in the derivative of the thermodynamic potential G with respect to the chemical potential, whose right and left limits are related to the two coexisting densities,

$$\rho_v=\left.\frac{\partial G}{\partial\mu}\right|_{\mu_c^-}<\left.\frac{\partial G}{\partial\mu}\right|_{\mu_c^+}=\rho_l. \tag{55}$$

Detecting a cusp in $G^{p=-1}$ leads, however, to a rather inaccurate determination of the phase boundaries. Instead it is much more convenient to look at the behavior along the staggered magnetization axis. In fact for $T<T_t$ the staggered susceptibility $\mathcal{C}_{cc}^{p=-1}(k=\pi)$ may vanish in a region of the staggered magnetization axis, which does not include the value $\varphi=0$ [see Fig. 2(a)]. Conversely, above the tricritical point [Fig. 2(b)], $\mathcal{C}^{p=-1}(k=\pi)$ vanishes in a region which always includes the value $\varphi=0$.

Therefore, the order parameter (i.e., the spontaneous staggered magnetization) varies continuously starting from zero along the Néel line, while along the liquid-gas coexistence curve it abruptly jumps from zero to a finite value when the coexistence curve is encountered (Fig. 2).

A. Blume Capel model

Figure 1 shows the phase diagram, in the ρ-T plane, of the Blume-Capel model obtained by integration of HRT equations (temperatures are measured in unit of $6\mathrm{J}/k_B$). For comparison, results from SCOZA of Grollau *et al.* [14,23] are also shown. The line of critical points (Néel line) ends at a tricritical point localized at $T_t=0.230\pm0.002$, $\rho_c\sim0.350\pm0.005$. In Table I we make a comparison with published results obtained with other methods. The two simulation results reported have been obtained by two different techniques: in Ref. [20] simulations were performed in the microcanonical ensemble while in [21] a geometric cluster Monte Carlo algorithm was employed. As it can be seen, our prediction for T_t is about 2.5% less then Deserno's simulation [20] while it agrees well with that of Heringa and Blöte [21]. Conversely, SCOZA results are closer to the results of

TABLE I. Comparison of tricritical point coordinates for the Blume-Capel model. Temperatures are in units of 6 J/k_B.

	T_t	ρ_c
HRT	0.230 ± 0.002	0.350 ± 0.005
SCOZA [14,23]	0.2360 ± 0.0006	0.345 ± 0.006
Simulation of Ref. [20]	0.2364 ± 0.0001	0.39
Simulation of Ref. [21]	0.2315 ± 0.0001	

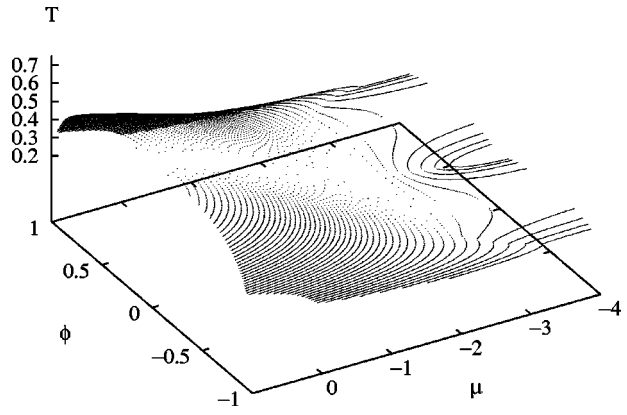

FIG. 3. Phase coexistence surface for the Blume-Capel model. Temperatures in are units of 6 J/k_B, μ in units of k_BT.

[20] than to those of [21]. Our estimate for the tricritical density agrees well with SCOZA estimate which is lower than the simulation result of Deserno.

In order to better understand the mechanism that allows one to localize the tricritical point we present in Fig. 3 a three-dimensional (3D) plot of the critical surface. As it can be seen, above T_t the critical surface is always centered around $\varphi=0$, while, below this temperature, for low values of the chemical potential, the surface does not include this value.

Figures 4 and 5 show the behavior of the order parameter (the spontaneous staggered magnetization) below and above the tricritical point showing the change from first order to second order in the character of the transition.

B. Lattice restricted primitive model

In Fig. 6 we show the HRT results for the phase diagram of the LRPM in the T-ρ plane. Predictions from SCOZA [14] and simulations [12,13] are also displayed for comparisons. In this section temperatures are measured in units of q^2/Dk_B. As for the Blume-Capel model there is a Néel line

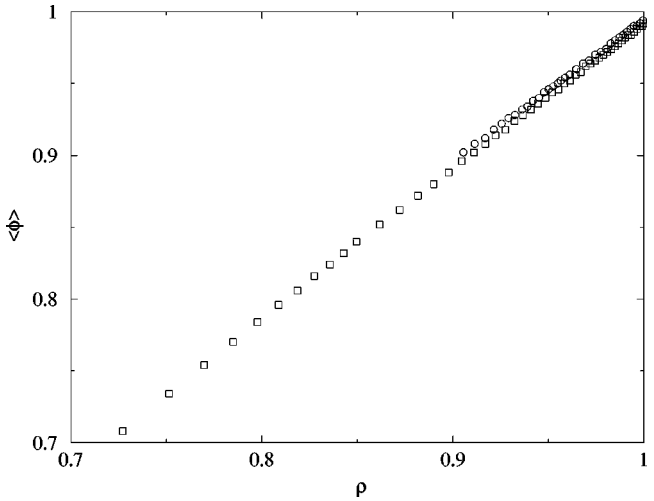

FIG. 4. Order parameter behavior for the Blume-Capel below the tricritical point. Temperatures in units of 6 J/k_B are 0.18 (circles) and 0.22 (squares).

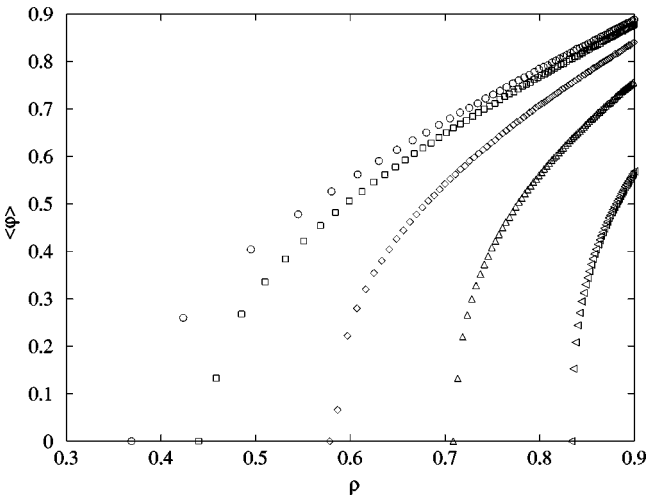

FIG. 5. Order parameter behavior for the Blume-Capel above the tricritical point. Temperatures in units of 6 J/k_B are (from left to right) 0.25, 0.30, 0.40, 0.50, and 0.60.

that ends at the tricritical point, which is localized at $T_t = 0.202 \pm 0.002$, $\rho_c \sim 0.380 \pm 0.005$. As it can be seen in Table II our estimate for the tricritical temperature deviates about 30% both from the simulation results by Panagiotopulos and Kumar [13] and Dickman and Stell [12]. However, as mentioned in Sec. III B, our interaction potential (42) is different from that used in simulations. Furthermore, as stated in [12], simulations have been performed only on small lattices and this could partially explain the discrepancies with our results. In order to check this aspect we tried to simulate the finite size effect by stopping the integration at a cutoff of the order $k \sim 2\pi/L$ which corresponds to

$$p \sim 1 - \frac{2\pi^2}{L^2}. \tag{56}$$

Even if for $L<30$ the localization of the tricritical point

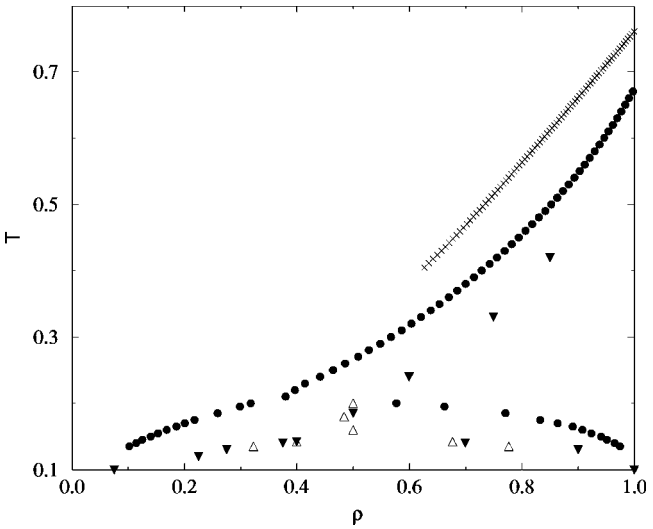

FIG. 6. Phase diagram in the T-ρ plane for the LRPM. Filled circles, HRT results; crosses, SCOZA data for the λ line; up triangles, simulation of Ref. [13]; down triangles, simulation of Ref. [12].

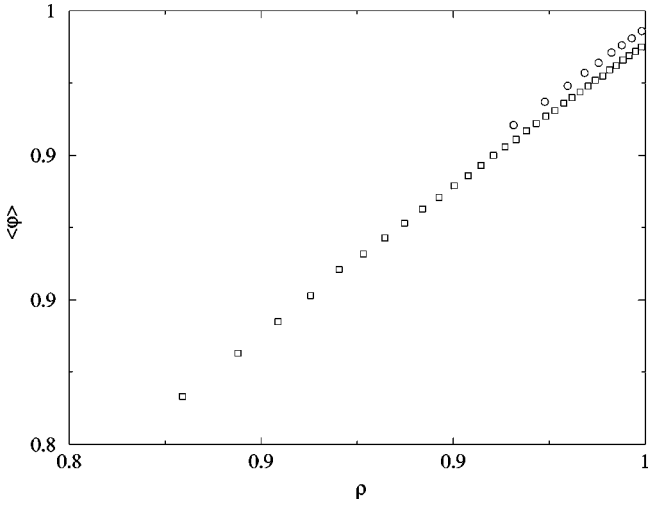

FIG. 7. Order parameter behavior for the LRPM below the tricritical point. Temperatures in units of q^2/Dk_B are 0.18 (circles) and 0.20 (squares).

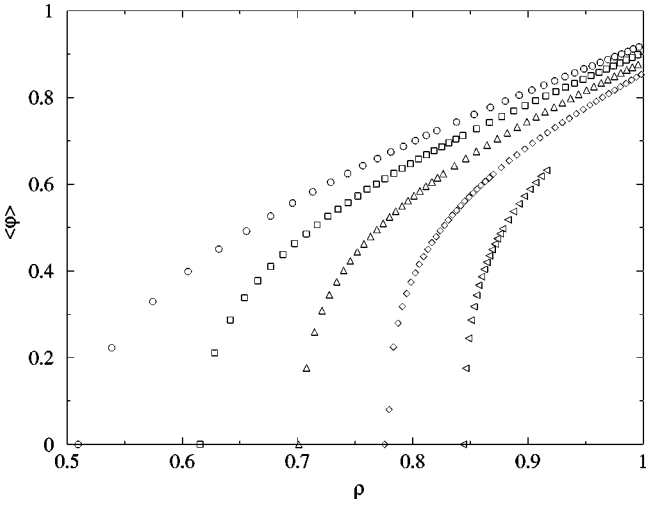

FIG. 8. Order parameter behavior for the LRPM above T_t. Temperatures in units of q^2/Dk_B are (from left to right) 0.25, 0.30, 0.35, 0.40, and 0.45.

becomes quite difficult, the tricritical temperature drifts to smaller values if the long wavelength fluctuations are neglected. In particular, for a lattice with $L=20$, we estimate a tricritical temperature of about 0.165. Our estimate of the tricritical density is in good agreement with the only available results of [12].

In Figs. 7 and 8 the results for the order parameter below and above the tricritical point are shown, respectively.

The mean-field-theory approach to Coulomb criticality developed by Fisher and co-workers [6] confirmed the important role played by the phenomenon of dipole association in determining the shape of the coexistence curve in the restricted primitive model of electrolytes.

In this approach, the density of dipoles ρ_d is estimated on the basis of the phenomenological picture by Bjerrum [7] who defined, in the low density regime, an ''association constant'' $K(T)$ describing the dipole formation process as a chemical reaction,

$$\rho_d \sim \rho_+ \rho_- K(T) \tag{57}$$

Due to the close analogy between the lattice and the continuum Coulomb gas, it is natural to expect that a similar phenomenon also occurs in the model we have studied. In order to assess the relevance of dipole formation in the low density region of the phase diagram of Fig. 6, we first have to identify a microscopic analog of ''dipole density:'' The simplest guess is to set

TABLE II. Comparison of tricritical point coordinates predictions for the LRPM. Temperatures are in units of q^2/Dk_B.

	T_t	ρ_c
HRT	0.202 ± 0.002	0.380 ± 0.005
Mean field [9,12]	0.299	0.333
Simulation of Ref. [12]	0.14	0.4
Simulation of Ref. [13]	0.15 ± 0.01	0.48 ± 0.02

$$\rho_d = \rho_{+-}(1) 2d, \tag{58}$$

where $\rho_{+-}(r)$ is the probability that two oppositely charged particles sit at distance r on the lattice and the proportionality factor $2d$ represents the number of distinct dipole orientations in an hypercubic, d-dimensional lattice. The correlation function $\rho_{+-}(1) = F_{+-}(1) + \rho_+(0)\rho_-(1)$ can be expressed in terms of the charge response alone if we assume that like charges do not occupy nearest neighbors sites $[\rho_{++}(1) \sim 0]$. This leads to the estimator for the dipole density we have adopted,

$$\rho_d = d[\langle \varphi \rangle^2 - F_{cc}(1)], \tag{59}$$

where $\langle \varphi \rangle$ is the order parameter. From definition (57) it follows that the association constant $K(T)$ can be identified with the low density limit of the expression

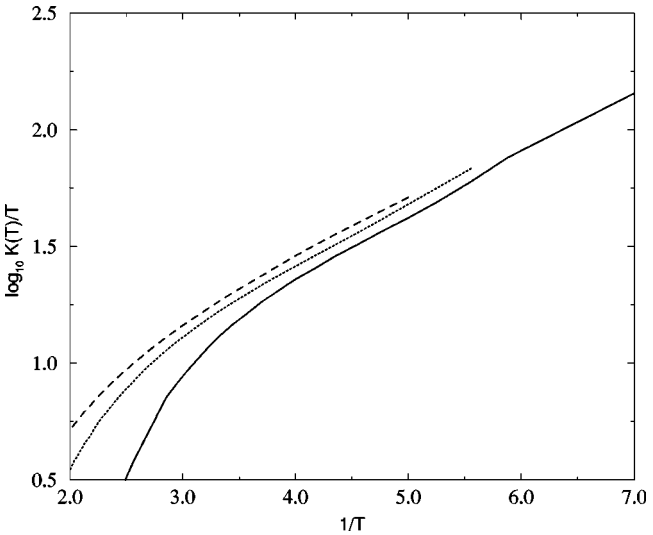

FIG. 9. Behavior of the dipole concentration constant vs temperature. Densities are (from below to up) 0.10, 0.15, and 0.20.

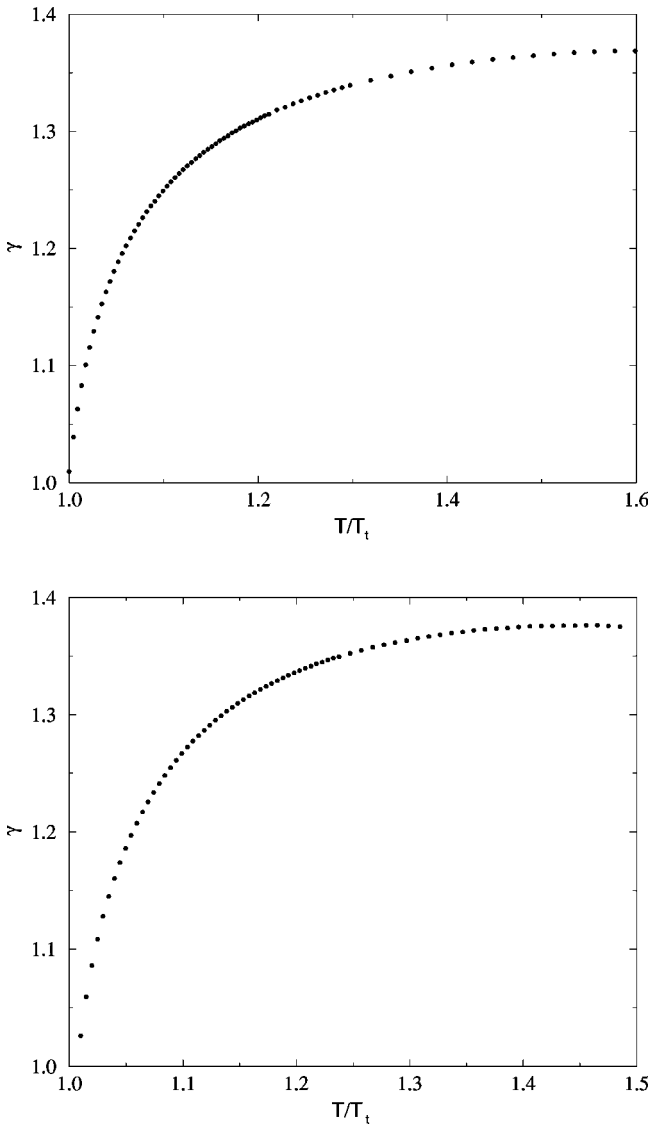

FIG. 10. Values of the asymptotic critical exponent γ vs temperature. Upper figure: results for the Blume-Capel model. Lower figure: results for the LRPM model. At high temperatures the exponent takes the value predicted by the Ising universality class with a Ornstein-Zernike closure ($\gamma=1.38$). Near T_t instead the exponent crosses over the mean-field value $\gamma=1.0$.

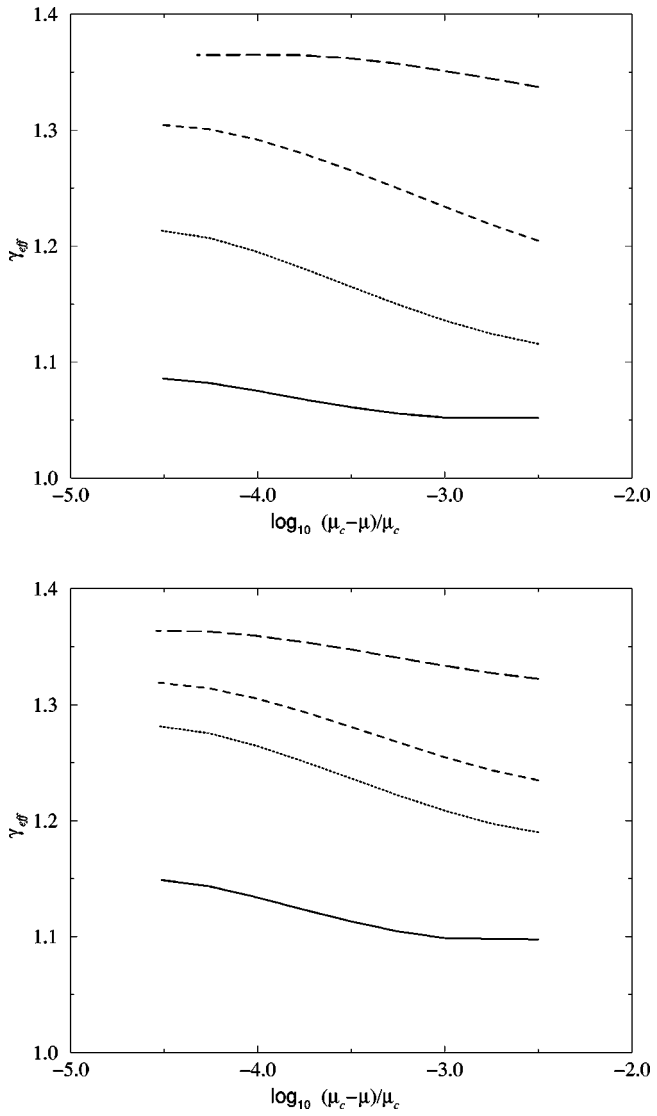

FIG. 11. Crossover from classical to Ising critical exponent along various isotherms (from below to up $T/T_t=1.0$, 1.05, 1.13,1.5 in both figures). In the upper figure we show the results for the Blume-Capel model. In the lower figure results for the LRPM model are displayed.

$$K(T)=4d\frac{\langle\varphi\rangle^2-F_{cc}(1)}{\rho^2}. \tag{60}$$

In the ''paramagnetic'' phase, the order parameter $\langle\varphi\rangle$ vanishes and the association constant is just proportional to the charge correlation function at nearest neighbors. According to the phenomenological approach, in the low density regions, the association process grows exponentially at low temperatures: $K(T)\propto Te^{1/T}$ [6]. In Fig. 9 we provide a logarithmic plot of $K(T)/T$ as a function of $1/T$ in the low density phase as obtained by the HRT approach. At low temperatures, the curves display the expected exponential behavior, showing that dipole association comes out naturally in our treatment with no need to include ''by hand'' the dipolar component to the Coulomb gas.

C. Critical behavior near the tricritical point

In this section we examine on the basis of the HRT equations, the critical properties of the two models we have studied. It is known that in the regions of the phase diagram characterized by a large staggered susceptibility, the HRT Eq. (15) simplifies and acquires a universal structure independent of the two-body interaction $\phi(k)$. As discussed in Ref. [16], the resulting asymptotic equation coincides with the one derived within the RG approach in local potential approximation. Scaling laws are therefore obeyed by our approximation with the critical exponents of the Ising universality class: $\gamma\sim1.38$ and $\eta=0$ at every critical point on the Neél line. At the tricritical point, the RG flow is instead

attracted by the Gaussian fixed point leading to classical critical behavior [22]: The singular part of the thermodynamic potential at fixed staggered field is given by

$$G(T,\mu)\sim u^{d/2}f(vu^{(d-4)/2}), \tag{61}$$

where $d=3$ is the space dimensionality, $f(x)$ is a universal scaling function, and the two fields (u,v) are linear combinations of the deviations of T and μ from their tricritical values. This scaling form implies that, at fixed temperature, the staggered susceptibility $F_{cc}(k=\pi)$ diverges as $|\mu_c-\mu|^{-\gamma}$ with $\gamma=1$. The shape of the liquid-vapor coexistence curve (in three dimensions) is instead governed by the exponent $\beta=1$ and displays the well known cusp of the λ line. This analytical result is compatible with the phase diagrams reported in Figs. 1 and 6 obtained by numerical integration of the HRT equations.

It is also interesting to investigate the nonuniversal crossover phenomena on the λ line when the tricritical point is approached. In particular, it is not clear whether the long range nature of the Coulomb potential severely affects the extent of the asymptotic critical region or not. In order to clarify this point, we have extracted an effective critical exponent γ_{eff} by fixing the temperature T larger than the tricritical value and computing the staggered susceptibility as a function of the reduced chemical potential $(1-\mu/\mu_c)$ in the range 10^{-3}–10^{-5}. The plots of the effective exponents for the two models are shown in Fig. 10 and indicate a smooth crossover between the asymptotic Ising value, attained at the highest temperatures and the classical limit reached at the tricritical point. The large difference in the range of the potential for the two models we have examined does not have significant consequences on the extent of the near-critical region, probably because the relevant fluctuations occur at $k\sim\pi$, a region where the two microscopic potentials behave in a quite similar way. This numerical analysis shows that the asymptotic critical region around a point on the Neél line shrinks considerably at temperatures few percent larger than the tricritical temperature suggesting that, in this region of the phase diagram, an accurate experimental determination of the true critical exponents should require a very close approach to the λ line.

In Fig. 11 we present the behavior of γ_{eff} at a fixed temperature as a function of the chemical potential for both models. As shown, near the tricritical temperature the Ising critical exponent can be detected only very close to the λ line $(1-\mu/\mu_c<10^{-5})$. Increasing the temperature instead extends the crossover region to the higher value of the reduced chemical potential $(1-\mu/\mu_c\sim10^{-4})$. No significant differences in the crossover behavior of the two models have been noted.

V. CONCLUSIONS

In this work we have developed a formulation of the HRT for the study of symmetric binary mixtures with an interacting potential of the type $\phi_{1,1}=-\phi_{1,2}$. This formulation has the advantage of allowing for the elimination of one density variable from the general equation for binary mixtures. Further simplification has been possible because we studied the system at fixed chemical potential rather then at fixed density leading to a hierarchy of evolution equations which contains only concentration correlation functions.

In order to obtain quantitative results to be compared with predictions of other methods we applied the theory to the study of two important lattice models using a single closure relation for the two-point correlation function that does not implement the core condition. The numerical solution of the resulting equation allowed us to derive the phase diagram of both models, Figs. 1 and 6. For the Blume-Capel model, predictions for the tricritical temperature and densities are in good agreement with both simulations and SCOZA results (Table I). Results for the tricritical temperature of the LRPM (Table II) instead do not agree so well with available simulations. This discrepancy can be ascribed to two reasons.

(1) The first is that the interaction potential of Eq. (9) reproduces the Coulomb potential used in simulations only at large distances.

(2) The second concerns simulations which were performed on small lattices ($L\leqslant20$) without any finite size scaling analysis.

In the two models we examined, both the Néel and the liquid-vapor transition were triggered by charge fluctuations at $k=\pi$, which led to the formation of strongly correlated pairs of opposite charge. In fact, the low-density, low-temperature regime of the LRPM can be interpreted on the basis of a dipole gas, as pointed out by Bjerrum and confirmed by our RG investigation.

The generalization of this approach to LRPM with extended core, already studied using Monte Carlo [13], is an interesting program that deserves future investigation. The HRT evolution equations may be obtained also in this case with a noticeable difference regarding the relevant wave vector for charge fluctuations, which will be shifted to smaller values, in agreement with the field theory developed by Ciach and Stell [9,10]. However, according to our approach, the ''Néel'' transition line which originates from the close packing limit would now be described by an order parameter with a larger number of components, as usual in lattice models with competing interactions [24]. By increasing the core radius, this phase transition is likely to become first order, thereby mimicking a freezing line. However, the mechanism leading to the development of a genuine liquid-vapor critical point at low density, without any visible singularity in the dielectric function, still remains a crucial unsolved issue for future studies.

ACKNOWLEDGMENTS

We want to thank S. Grollau, E. Kierlik, M. L. Rosinberg, and G. Tarjus for the data of SCOZA reported in Figs. 1 and 6.

[1] M. E. Fisher, J. Stat. Phys. **75**, 1 (1994).
[2] G. Stell, J. Stat. Phys. **78**, 197 (1995).
[3] T. Narayanan and K. S. Pitzer, J. Chem. Phys. **102**, 8118 (1995); R. R. Singh and K. S. Pitzer, *ibid.* **92**, 6775 (1990); K. C. Zhang *et al.*, *ibid.* **97**, 8692 (1992).
[4] P. W. Debye and E. Hückel, Phys. Z. **24**, 185 (1923).
[5] G. Stell, K. C. Wu, and B. Larsen, Phys. Rev. Lett. **37**, 1369 (1976).
[6] M. E. Fisher and Y. Levin, Phys. Rev. Lett. **71**, 3826 (1993).
[7] N. Bjerrum, K. Dan. Vidensk. Selsk. Mat. Fys. Medd. **7**, 1 (1923).
[8] J. S. Høye and G. Stell, J. Stat. Phys. **89**, 177 (1997).
[9] A. Ciach and G. Stell, J. Mol. Liq. **87**, 255 (2000).
[10] A. Ciach and G. Stell, J. Chem. Phys. **114**, 382 (2001).
[11] G. Stell, in *New Approaches to Problems in Liquid-State Theory*, edited by C. Caccamo, J. P. Hansen, and G. Stell (Kluwer Academic, Dordrecht, 1999).
[12] R. Dickman and G. Stell, in *Simulation and Theory of Electrostatic Interactions in Solutions*, edited by L. R. Pratt and G. Hummer (AIP, Woodbury, NY, 1999), pp. 225–249.
[13] A. Z. Panagiotopoulos and S. K. Kumar, Phys. Rev. Lett. **83**, 2981 (1999).
[14] S. Grollau, Ph.D. thesis, Université Pierre et Marie Curie, Paris, 2001.
[15] D. Pini, A. Parola, and L. Reatto, J. Stat. Phys. **72**, 1179 (1993).
[16] A. Parola and L. Reatto, Adv. Phys. **44**, 211 (1995).
[17] A. Parola and L. Reatto, Phys. Rev. A **44**, 6600 (1991).
[18] W. H. Press, B. P. Flannery, S. A. Teukolsky, and W. T. Vetterling, *Numerical Recipes* (Cambridge University Press, Cambridge, 1986).
[19] W. F. Ames, *Numerical Methods for Partial Derivative Equations* (Academic Press, New York, 1977).
[20] M. Deserno, Phys. Rev. E **56**, 5204 (1997).
[21] J. R. Heringa and H. W. J. Blöte, Phys. Rev. E **57**, 4976 (1998).
[22] I. D. Lawrie and S. Sarbach, in *Phase Transition and Critical Phenomena*, edited by C. Domb and M. S. Green (Academic Press, London, 1984), Vol. 9.
[23] S. Grollau, E. Kierlik, M. L. Rosinberg, and G. Tarjus, Phys. Rev. E **63**, 041111 (2001).
[24] S. Krinsky and D. Mukamel, Phys. Rev. B **16**, 2313 (1977).